Intrinsic coherence time of trions in monolayer MoSe_{2} measured via two-dimensional coherent spectroscopy

Michael Titze, Bo Li, Xiang Zhang, Pulickel M. Ajayan, and Hebin Li

Phys. Rev. Materials **2**, 054001 — Published 10 May 2018

DOI: 10.1103/PhysRevMaterials.2.054001

Intrinsic coherence time of trions in monolayer $MoSe_2$ measured via two-dimensional coherent spectroscopy

Michael Titze,[1] Bo Li,[2,3] Xiang Zhang,[2] Pulickel M. Ajayan,[2] and Hebin Li[1,*]

[1]*Department of Physics, Florida International University, Miami, Florida 33199*
[2]*Department of Materials Science and NanoEngineering, Rice University, Houston, Texas 77005*
[3]*Department of Mechanical Engineering, Villanova University, Villanova, Pennsylvania 19085*

Quantum coherence and its dynamics in monolayer transition metal dichalcogenides (TMDs) are essential information to fully control valley pseudospin for valleytronics applications. Experimental understanding of coherence dephasing dynamics has been limited for excitons and largely unexplored for trions in monolayer TMDs. Here we use optical two-dimensional coherent spectroscopy to measure the trion coherence dephasing time in monolayer $MoSe_2$ by analyzing the homogeneous linewidth. An intrinsic coherence time of 182 fs is extrapolated from the excitation density and temperature dependence measurement. The results show that trion-trion and trion-phonon interactions strongly affect the coherence dephasing time, while the intrinsic coherence time at zero excitation and zero temperature is primarily limited by the pure dephasing due to defect states. Our experiment also confirms optical two-dimensional coherent spectroscopy as a reliable technique for studying valley quantum dynamics in two-dimensional layered materials.

I. INTRODUCTION

Monolayer transition metal dichalcogenides (TMDs), as a class of semiconducting two-dimensional (2D) crystals, have unique electronic and optical properties that can lead to novel applications in electronics, optoelectronics[1] and valleytronics[2]. In particular, the ability to selectively address one of the nonequivalent K valleys[3] allows manipulation of the valley pseudospin degree of freedom[4] for valleytronics which aims to use valley indices as carriers for information processing[5–10]. To realize the full quantum control of the valley pseudospin such that the pseudospin vector can be steered throughout the entire Bloch sphere[2], it is required to control dynamics of not only valley population but also quantum coherence which is a coherent superposition of two states.

In general, a quantum state can be represented by a density matrix in which the diagonal matrix elements are associated with populations in each state, while the off-diagonal matrix elements indicate quantum coherences. Since the full information on a quantum system is encoded as matrix elements in the density matrix, manipulating a quantum system for applications such as quantum information processing[11] must include off-diagonal elements, thus quantum coherence. Moreover, quantum coherence plays a crucial role in determining many properties and functionalities of various materials including chemical and biological systems[12]. Experimentally confirmed understanding of quantum coherence in monolayer TMDs is essential for engineering these materials to realize potential applications.

Quantum coherence can be created by an optical excitation of a laser pulse and generally decays over time, which is referred to as dephasing or decoherence. Coherence dephasing processes are a critical part of carrier dynamics in semiconductors. Quantum dynamics of carriers are characterized by two fundamental time scales: population decay time T_1 and coherence dephasing time T_2. These two time parameters are related through $\frac{1}{T_2} = \frac{1}{2T_1} + \frac{1}{T_2^*}$, where T_2^* is the pure dephasing time due to processes other than population decay. The upper limit on T_2 is given by $2T_1$ in the case that quantum coherence is lost only through population decay. However, in semiconductors coherence dephasing time is usually dominated by multiple pure dephasing processes. Experimental measurement of T_2 is essential to characterize quantum coherence. The population decay time T_1 in monolayer TMDs has been studied in a variety of time-resolved experiments[13–21]. Compared to T_1, there are two major differences in measuring T_2. The experiment must be a coherent process such as transient four-wave mixing (TFWM) in which a coherence is generated and measured. The coherence dephasing time can be related to the homogeneous linewidth Γ through $T_2 \propto 1/\Gamma$. In an inhomogeneously broadened system, homogeneous and inhomogeneous contributions in the linewidth must be separated and measured.

Optical two-dimensional coherent spectroscopy (2DCS)[22,23] provides an effective tool to measure the coherence dephasing time T_2 through homogeneous linewidth in an inhomogeneous system. The experiment is based on a three-pulse TFWM process in which a coherence is created and evolves. The dynamics of the coherence can be retrieved from spectra even in the presence of strong inhomogeneous broadening. In a 2D spectrum, homogeneous and inhomogeneous linewidths are separated and can be measured along the cross-diagonal and diagonal directions[24], respectively. Optical 2DCS has been widely used to study various systems such as atomic vapors[25,26], photosynthetic complexes[27,28], and semiconductor quantum wells[29–32] and dots[33,34]. More recently, utilizing optical 2DCS to study monolayer TMDs has been pioneered by X. Li and coauthors[35–39]. However, optical 2DCS measurements on monolayer TMDs remain extremely challenging due

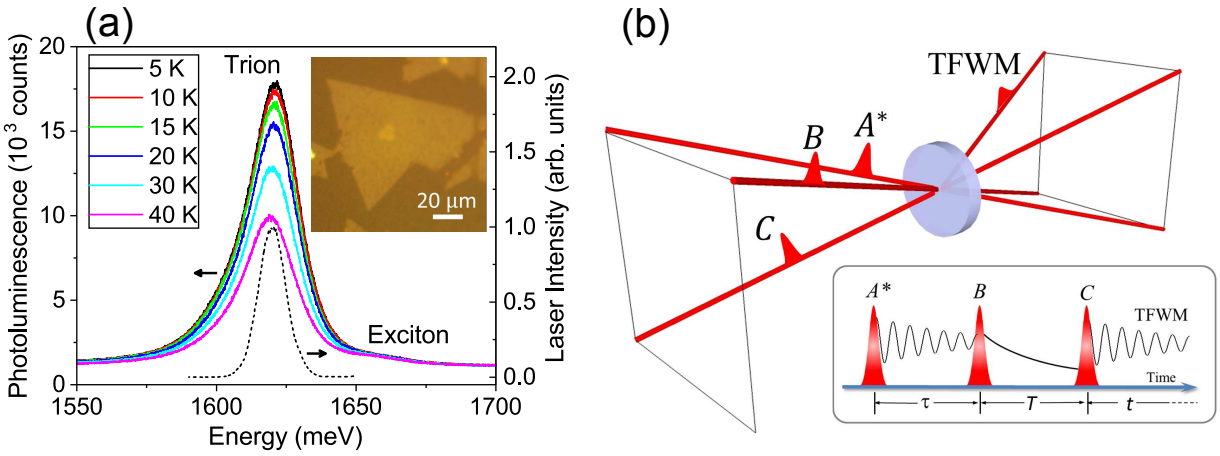

FIG. 1: (a) PL spectra (solid lines) at various temperatures from 5 to 40 K and the laser spectrum (dashed line) used in 2DCS measurements. The inset is an optical image of a $MoSe_2$ monolayer. (b) A schematic of the 2DCS experiment in the box geometry. The inset shows the time ordering of excitation pulses.

to weak third-order nonlinear signal from monolayer samples.

In this letter, we report a 2DCS experiment on monolayer $MoSe_2$ in which the coherence dephasing time T_2 is extracted from homogeneous linewidth for the trion resonance. Trions are charged excitons that can form in the presence of excess charges[40,41]. In monolayer TMDs, trions have high binding energies[42–44] which allow them to form even at room temperature. Trions also significantly influence optical and electronic properties of layered TMDs, such as modifying the overall photoluminescence (PL) spectrum[43] and reducing the conductivity[45]. Excitons and trions are coupled through relaxation, phonon-excited upconversion[46], and even coherent interaction[47]. Their interplay has important implications in many applications. It is critical to understand both exciton and trion dynamics. Trion formation[48] and relaxation dynamics[49,50] in monolayer TMDs have been recently studied using time-resolved techniques. Our 2DCS experiment focuses on the coherence dephasing time of trions. The homogeneous linewidth is extracted from 2D spectra for different excitation densities and sample temperatures to extrapolate the residual homogeneous linewidth at zero excitation density and zero temperature. For a monolayer $MoSe_2$ sample, we obtained an residual homogeneous linewidth of $\Gamma = 3.6 \pm 0.04$ meV, corresponding to an intrinsic coherence dephasing time of $T_2 = 182 \pm 2$ fs.

II. EXPERIMENT AND RESULTS

Monolayer $MoSe_2$ used in our measurements was synthesized on a Si substrate by chemical-vapor-deposition (CVD)[51] and subsequently transferred to an anti-reflection (AR) coated quartz plate. The transparent substrate allows transmission measurements and the AR coating reduces the scattering of excitation pulses to improve the signal-to-noise ratio. Monolayer flakes are equilateral triangles with size ranging from 10 to 100 μm, as shown in Fig. 1(a). The sample was cooled in a liquid helium cryostat for low temperature experiments. Prior to 2DCS measurement, the PL spectra were taken with a 532-nm excitation at different sample temperatures, as shown in Fig. 1(a). The dominating feature at around 1620 meV corresponds to the trion resonance, while the exciton peak at around 1655 meV is much weaker. Based on the resonance energy revealed in the PL spectra, the center of the laser spectrum (dashed line in Fig. 1(a)) is tuned to 1620 meV for 2DCS measurements.

A non-colinear 2DCS approach[22] with active phase locking was used to acquire 2D spectra of monolayer $MoSe_2$. The experimental schematic is shown in Fig. 1(b). Briefly, three excitation pulses A^*, B, and C with wave vectors $-\mathbf{k}_A$, $\mathbf{k}_B$, and $\mathbf{k}_C$ converge onto the sample and generate a TFWM signal in the direction $\mathbf{k}_S = -\mathbf{k}_A + \mathbf{k}_B + \mathbf{k}_C$. In the time domain, the excitation process by the pulse sequence in Fig. 1(c) can be understood by modeling the trion resonance as an inhomogeneously broadened two-level system. For a two-level system and the phase-matched direction $\mathbf{k}_S$, pulse A^* excites a coherence between the excited and ground states, pulse B converts the coherence to a population and forms a population grating, and pulse C scatters off the grating to give a TFWM signal. A 2D spectrum is obtained by scanning τ and Fourier-transforming the signal with respect to τ and t. Since the coherence generated by pulse A^* dephases during τ, the obtained 2D spectra contain the coherence dephasing dynamics in cross-diagonal linewidth[24].

For a monolayer sample on a thick substrate (1-mm quartz plate in our experiment), the third-order nonlinear TFWM signal is usually overwhelmed by the scattering of laser beams on the substrate, leading to a poor signal-to-noise ratio (SNR). To overcome this difficulty, the quartz plate is AR-coated to reduce the back reflection. More-

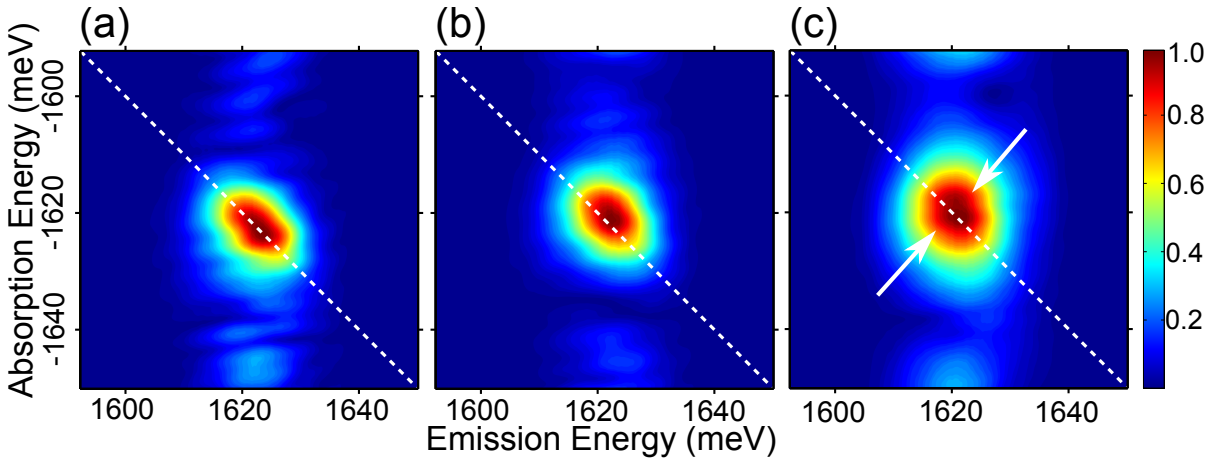

FIG. 2: 2D spectra of the trion resonance in monolayer $MoSe_2$ at a sample temperature of 5 K. The spectra are obtained at an excitation density of (a) $N = 6.5 \times 10^{11}$ cm^{-2}, (b) $N = 1.95 \times 10^{12}$ cm^{-2}, and (c) $N = 3.90 \times 10^{12}$ cm^{-2}.

over, we implement a phase-cycling technique[52] in which the phases of pulses A^* and B are toggled by liquid crystal phase modulators such that a series of spectra can be acquired to cancel out the background noise but not the signal. This method significantly improves the SNR and is essential to obtain reliable 2D spectra of monolayer $MoSe_2$.To ensure the acquired 2D spectra are indeed due to the third-order nonlinear TFWM signal rather than the linear scatter of laser beams, we measured the power dependence of the signal to verify the nonlinear feature.

Typical 2D spectra of the trion resonance in monolayer $MoSe_2$ at 5 K are shown in Fig. 2 for three different excitation densities. The spectral amplitude is plotted with the maximum normalized to 1. The excitation density is calculated from the pulse energy with a laser spot size of 70 μm in diameter and an absorption of 10%. The laser spectrum, as shown in Fig. 1(a) as the dashed line, is tuned to the trion resonance but narrower than the inhomogeneously broadened trion resonance. Generally diagonal linewidth is determined by the inhomogeneous broadening[24], while in our experiment it is limited by the laser spectrum. Homogeneous linewidth is associated with the cross-diagonal direction, as denoted by the arrows in Fig. 2(c). As the excitation density increases, the diagonal linewidth remains almost the same, while the cross-diagonal linewdith increases indicating a faster coherence dephasing due to the effect of excitation induced dephasing (EID)[53]. Investigating the instrinsic homogeneous linewidth without the effect of EID requires a power dependence measurement.

The homogeneous linewidth is extracted by analyzing cross-diagonal slices. In our experiment, the analysis requires to account for the finite pulse duration of excitation pulses. In the cases where the time scale to be measured is much longer than the laser pulse duration, the pulse can be approximated with a Delta function and the cross-diagonal slice can be fit with the square root of a Lorentzian profile[24] for a strongly inhomogeneously broadened 2D spectrum. However, if the pulse duration is comparable to the time scale of interest, which is the case in this study, the Delta pulse approximation is no longer valid and the resulting spectral shape is significantly affected by the pulse duration in addition to the sample response. The effects of a finite pulse duration in 2D spectral lineshape has been accounted for in theoretical models[54,55]. Briefly, the finite pulse duration leads to a modification of the square root Lorentzian profile in cross-diagonal slices. We used this finite pulse model to fit our spectra to extract the homogeneous linewidth Γ. The model and fitting are described in Appendix A. As an example, fitting of a cross-diagonal slice in the 2D spectrum in Fig. 2(c) is shown in Fig. 3(a), where the black and red lines are data and fit, respectively. The fitting gives a homogeneous linewidth of $\Gamma = 4.50 \pm 0.04$ meV which corresponds to a coherence time of $T_2 = 146 \pm 2$ fs. The timescale of measured T_2, which is comparable to the excitation pulse duration (Gaussian width $\sigma = 100$ fs), confirms the requirement to account for the finite pulse duration in analyzing the spectra.

The 2D spectra in Fig. 2 demonstrate significant effects of EID which leads to the broadening in homogeneous linewidth at higher excitation densities[53]. To systematically study EID in monolayer $MoSe_2$, the 2DCS measurement and linewidth analysis are repeated with various laser powers to obtain the homogeneous linewidths at different excitation densities. The homogeneous linewidths acquired at a sample temperature of 5 K are plotted in Fig. 3(b) for excitation densities across about an order of magnitude ($10^{11} \sim 10^{12}$ cm^{-2}). The error bars represent standard deviations that are calculated from multiple measurements at each data point. The measured homogeneous linewidth exhibits a linear dependence on the excitation density. Thus we fit the data with a linear function $\Gamma = \Gamma_0 + n \cdot \Gamma_{EID}$, where Γ_0 is the zero-excitation linewidth, n is the excitation den-

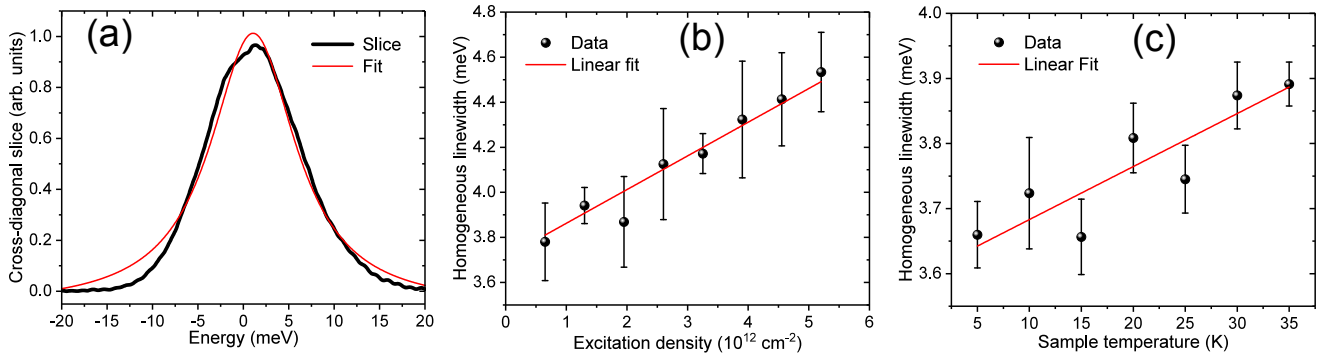

FIG. 3: (a) A cross-diagonal slice (black) in 2D spectrum in Fig. 2(c) and the fit (red) based on the finite pulse model. (b) The excitation density dependence of the measured homogeneous linewidth at 5 K. (c) The temperature dependence of the extrapolated homogeneous linewidth at zero excitation density. The red lines are linear fits.

sity, and Γ_{EID} is the rate of change in the homogeneous linewidth with the excitation density. The fitting routine uses the instrumental weighting that accounts for the error bars. The fit (red line) in Fig. 3(b) yields $\Gamma_0 = 3.71 \pm 0.04$ meV and $\Gamma_{EID} = 1.5 \times 10^{-13}$ meV·cm^2 for a sample temperature of 5 K. This observation indicates the contribution of trion-trion interactions to the coherence dephasing process in monolayer $MoSe_2$.

Furthermore, we repeat the excitation density dependence measurement for every increase of 5 K in temperature up to 35 K. The 2DCS signal starts to vanish and is not measurable above 35 K. The data for temperatures other than 5 K are included in Appendix B. The homogeneous linewidths at all measured temperatures show a linear dependence on the excitation density, so they are fit linearly to extrapolate the corresponding zero-excitation linewidths which are plotted in Fig. 3(c). This temperature dependence can be fit with a linear function $\Gamma_0 = \Gamma_{00} + T_s \cdot \alpha$, where Γ_{00} is the homogeneous linewidth at zero temperature and zero excitation, T_s is the sample temperature, and α is the rate of change in the zero-excitation linewidth with the sample temperature. The fit (red line) in Fig. 3(c) gives $\Gamma_{00} = 3.60 \pm 0.04$ meV and $\alpha = 8.2 \pm 1.6$ μeV/K. The zero-excitation linewidth increases with temperature, indicating that trion-phonon interactions also contribute to the coherence dephasing process in monolayer $MoSe_2$. The linear dependence on temperature suggests that the phonon interaction is primarily due to acoustic phonons[58]. The rate of increase in homogeneous linewidth due to the interaction with acoustic phonons is comparable to that of excitons in quantum wells[58] but is much smaller compared to excitons in monolayer WSe_2[35], MoS_2[57], WS_2 and $MoSe_2$[59], indicating that the phonon interaction with trion is weaker than exciton. We speculate that trions have stronger screening effects compared to excitons. However, the exact mechanism of weaker interaction with phonon is not clear in our experiment and can be an interesting topic for further studies.

III. DISCUSSION

The excitation density and temperature dependence data allow us to eliminate the effects of trion-trion and trion-phonon interactions in the coherence dephasing process by extrapolating a residual homogeneous linewidth at zero excitation and zero temperature. The obtained linewidth $\Gamma_{00} = 3.60 \pm 0.04$ meV corresponds to an intrinsic coherence dephasing time $T_2 = 182 \pm 2$ fs for the trion resonance in monolayer $MoSe_2$. Several experiments have been reported on directly measuring the coherence dephasing time of excitons[35,57] and trions[36,39] in monolayer TMDs by using either 2DCS or time-integrated four-wave mixing. Their results along with our current measurement are summarized in Table I. The trion coherence time was previously measured at a particular excitation density and a particular sample temperature. For excitons, the excitation and temperature dependence was studied to determine a coherence dephasing time at a few hundred fs. Our measurement of T_2 on the trion resonance is at the same order of magnitude but shorter than the measured T_2 of excitons in monolayer $MoSe_2$. The measured coherence dephasing time depends strongly on the excitation density and temperature. The intrinsic T_2 extrapolated from the dependence data provides a direct comparison of effects on coherence due to intrinsic properties of the sample, such as composition, defect level, and substrate. Moreover, the rates of change in the homogeneous linewidth with the excitation density and temperature reveal information about exciton/trion interactions with exciton/trion and with phonon. Our experiments along with the previous work[35] demonstrate that 2DCS provides reliable and systematic direct measurements of coherence dephasing time in monolayer TMDs, making it possible for further studies of microscopic mechanisms of coherence dephasing processes and relevant material parameters.

At a finite excitation density and temperature, tion-trion and trion-phonon interactions contribute to the coherence dephasing process. They play a similar role as exciton-exciton and exciton-phonon interactions

TABLE I: The reported results of direct measurements of the coherence dephasing time in various monolayer TMDs.

Material	Resonance	T_2	Temperature	Excitation	Method	Reference
WSe_2	Exciton	410 ± 50 fs	zero	zero	2DCS	[35]
WSe_2	Exciton	279 fs	5 K	$\sim$nJ/cm^2	TIFWM	[57]
MoS_2	Exciton	293 fs	zero	zero	TIFWM	[57]
$MoSe_2$	Exciton	394 fs	5 K	$\sim$nJ/cm^2	TIFWM	[57]
$MoSe_2$	Trion	510 ± 70 fs	20 K	$\sim \mu$J/cm^2	2DCS	[36,39]
$MoSe_2$	Trion	182 ± 2 fs	zero	zero	2DCS	This work

for the exciton coherence dephasing, as previously discussed[35,57]. However, there is a substantial residual homogeneous linewidth (about 80% of the largest linewidth in our measurements) at zero excitation and zero temperature, indicating an intrinsic coherence dephasing time that is independent of the pure dephasing caused by trion-trion and trion-phonon interactions. Considering that the upper limit on the coherence dephasing time is set by $2T_1$ when there is no pure dephasing process (i.e. $1/T_2^* = 0$), the intrinsic coherence dephasing time is mostly determined by the population decay. Previous homogeneous linewidth studies on excitons in WSe_2[35], $MoSe_2$ and WS_2[59] have confirmed the limiting role of T_1, while the responsible population decay is attributed to different microscopic processes in tungsten- and molybdenum-based TMDs. In WSe_2 and $MoSe_2$, the limiting process is the radiative decay[35,59], while the decay into dark excitonic states[59] is the determining mechanism in WS_2. It was also shown that the radiative decay does not introduce additional pure dephasing since the residual homogeneous linewidth was measured exactly half the population decay rate in WSe_2. To understand the microscopic origin of the intrinsic coherence dephasing time of trion in monolayer $MoSe_2$, we compare the present T_2 measurement to the pump-probe data[49] of the trion population decay dynamics in $MoSe_2$. As we previously reported[49], the trion population displays a bi-exponential decay and the fast decay process is attributed to the population trapping by defect states assisted by Auger scattering. The fast decay time at a low excitation density (1.8×10^{12} cm^{-2}) and temperature (10 K) is about 6 ps which is much longer than the measured intrinsic coherence dephasing time. This suggests that the trapping by defect states leads to not only a fast population decay but also an even faster pure dephasing of coherence which determines the intrinsic coherence dephasing time of trion in monolayer $MoSe_2$. This pure dephasing process could be the coherence loss due to trion scattering with defect states before the trions are trapped by defects. Since defect states significantly affect the population decay time and coherence dephasing time, both timescales can be potentially manipulated by engineering defects[60] in monolayer TMDs.

IV. SUMMARY

In summary, we have measured the coherence dephasing time of trions in monolayer $MoSe_2$ by using optical 2DCS. The measurements were taken at various excitation densities and sample temperatures. The excitation and temperature dependence reveals that trion-trion and trion-phonon interactions have significant influence on the coherence dephasing dynamics. We further extrapolated the intrinsic coherence time at zero excitation and zero temperature and found it is not limited by the population decay time. It is suggested that additional pure dephasing introduced by scattering of defect states is the limiting mechanism for the intrinsic dephasing time of trions in monolayer $MoSe_2$. So defect engineering could modify the trion dynamics in monolayer TMDs. The measured intrinsic coherence time here is specific to our particular sample which happens to be heavily doped. The valley coherence dynamics are strongly dependent on sample parameters such as impurity level, defects, substrate, and strain. Our experiment demonstrated optical 2DCS as a reliable technique for systematic studies of quantum coherence dynamics in 2D materials and dependence of quantum coherence on various material parameters.

Acknowledgments

The authors thank C.L Smallwood for discussion on data analysis and G. Moody for discussion on experiments. The work at FIU is partially supported by ARO grant number W911NF-17-1-0497.

Appendix A: Fitting a cross-diagonal slice

This appendix briefly discusses how a cross-diagonal slice of a 2D spectrum is fit when the coherence dephasing time is on the same order as the pulse duration. In order to simplify the calculation, only the case of a two-level system with ground state $|0\rangle$ and excited state $|1\rangle$ is considered. A detailed treatment can be found in Refs[54,55]. The discussion here is adapted from[54].

Starting with a semi-classical model and solving the optical Bloch equation perturbatively yields the n-th or-

der density matrix element

$$\rho_{ij}^{(n)}(t) = -\frac{i}{\hbar}\int_{-\infty}^{t}[\hat{V}(t'),\hat{\rho}^{(n-1)}]_{ij}e^{-i\Omega_{ij}(t-t')}dt' \quad \text{(A1)}$$

where $i,j = 0,1$, and

$$\Omega_{ij} = \begin{cases}\omega_{ij} - i\Gamma & \text{if } i \neq j \\ -i\gamma & \text{if } i = j\end{cases} \quad \text{(A2)}$$

with ω_{ij} being the transition frequncy, Γ being the coherence dephasing rate, and γ being the population decay rate. The interaction Hamiltonian $V(t)$ contains the electric field and is given as

$$V(t) = -\mu_{01}[E(t)e^{i(\mathbf{k}\cdot\mathbf{r}-\omega t)} + \text{c.c.}] \quad \text{(A3)}$$

with the transition dipole moment μ_{01}, the slowly varying envelope of the electric field $E(t)$, the wave vector $\mathbf{k}$, and the carrier frequency ω.

Assuming that the pulses have transform limited Gaussian shape which is a good approximation to the experimental pulse shape, the electric field envelope for each pulse is written as

$$E_i(t) = \frac{E_i^0}{\sqrt{2\pi}\sigma}e^{-\frac{(t-t_i)^2}{2\sigma^2}} \qquad i = A,B,C \quad \text{(A4)}$$

with σ being expressed through the intensity duration FWHM $\Delta t_{\text{FWHM}} = 2\sqrt{\ln(2)}\sigma$ and the t_i being the arrival times of the different pulses. Plugging in the pulse shapes and selecting only the signal in the phase-matched direction $\mathbf{k}_S = -\mathbf{k}_A + \mathbf{k}_B + \mathbf{k}_C$, equation (A1) gives

$$\begin{aligned}\rho_{01}^{(3)}(t) \propto & \mu_{01}^3\int_{-\infty}^{t}dt'''e^{-\frac{(t''')^2}{2\sigma^2}}e^{(i\omega_{01}-\Gamma)(t-t''')} \\ & \times\int_{-\infty}^{t'''}dt''e^{-\frac{(t''+T)^2}{2\sigma^2}}e^{-\gamma(t'''-t'')} \\ & \times\int_{-\infty}^{t''}dt'e^{-\frac{(t'+T-\tau)^2}{2\sigma^2}}e^{(-i\omega_{01}-\Gamma)(t''-t')} \quad \text{(A5)}\end{aligned}$$

Since only the relative arrival times matter in terms of the material response, the pulse arrival times have been replaced with the time-delays. The delays are defined as $\tau = t_B - t_A$, $T = t_C - t_B$ and $t = t - t_C$ where t is the emission time of the signal and the t_i correspond to the arrival time of pulse i. Performing a Fourier-transform along the t and τ direction yields the response function in the 2D frequency domain

$$\begin{aligned}S(\omega_\tau,\omega_t) &= \frac{S_0}{(\sqrt{2\pi}\sigma)^3}[1+\text{erf}(\frac{T+i\sigma^2(\omega_\tau+\omega_t-2\gamma)}{2\sigma})] \\ &\times\frac{i}{(\omega_\tau-\omega_0)+i\Gamma}\times\frac{i}{(\omega_t-\omega_0)+i\Gamma} \\ &\times e^{-\gamma T}e^{-\frac{\sigma^2(\omega_\tau-\gamma)^2}{2}}e^{-\frac{\sigma^2(\omega_t-\gamma)^2}{2}}e^{-\frac{\sigma^2\omega_T^2}{2}}, \quad \text{(A6)}\end{aligned}$$

where ω_τ and ω_t are the absorption and emission frequencies, ω_0 is the central frequency of the resonance, S_0 is the amplitude, and the error function is defined as $\text{erf}(x) = \frac{1}{\sqrt{\pi}}\int_{-\infty}^{x}e^{-t^2}dt$. Since $T = 0$ in all experiments presented, the equation can be written as

$$\begin{aligned}S(\omega_\tau,\omega_t) &= \frac{S_0}{(\sqrt{2\pi}\sigma)^3}[1+\text{erf}(\frac{i\sigma^2(\omega_\tau+\omega_t-2\gamma)}{2\sigma})] \\ &\times\frac{i}{(\omega_\tau-\omega_0)+i\Gamma}\times\frac{i}{(\omega_t-\omega_0)+i\Gamma} \\ &\times e^{-\frac{\sigma^2(\omega_\tau-\gamma)^2}{2}}e^{-\frac{\sigma^2(\omega_t-\gamma)^2}{2}}e^{-\frac{\sigma^2\omega_T^2}{2}}. \quad \text{(A7)}\end{aligned}$$

The effect of excitation with a finite pulse compared to excitation with a Delta pulse can be understood in the frquency domain as bandwidth limitation. While a Delta pulse contains equal spectral power for arbitrarily high and low frequencies, a finite pulse has a certain bandwidth, which is typically non-uniform in the spectral domain. The finite pulse effect is mathematically described by the convolution integral between the signal shape and the excitation pulse shape.

In order to fit a cross-diagonal slice, the full dataset is interpolated to a 2D matrix. The cross-diagonal slice through the resonance energy at point $(1620\text{meV}, 1620\text{meV})$ is taken from a 2D spectrum and fit to equation (A7). The fitting parameters are the signal amplitude S_0, the resonance frequency $\omega_{10} = -\omega_{01}$, the population decay rate γ, and the coherence dephasing rate Γ. Furthermore we include an offset in the fitting which is due to the experimental background being nonzero and does not appear in equation (A7).

Appendix B: Excitation density dependence of homogeneous linewdith at various temperatures

In addtion to the excitation density dependence of homogeneous linewidth at a temperature of 5 K, as shown in Fig. 3(b) in the main text, similar measurments are done for every increase of 5 K up to 35 K. The results for other temperatures are shown in Fig. 4. The data points are obtained from arithmetically averaging the homogeneous linewidth extracted from five or more independent measurements. The error bars are the corresponding standard deviations and are used in the linear fit as instrumental weights on the data points.

The homogeneous linewidth increases linearly with the excitation density at all temperatures. The data are fit to a linear function to extrapolate the homogeneous linewidths at zero excitation density. The obtained fitting parameters for all temperatures are plotted in Fig. 3(c) to extrapolate the homogeneous linewidth at zero excitation and zero temperature.

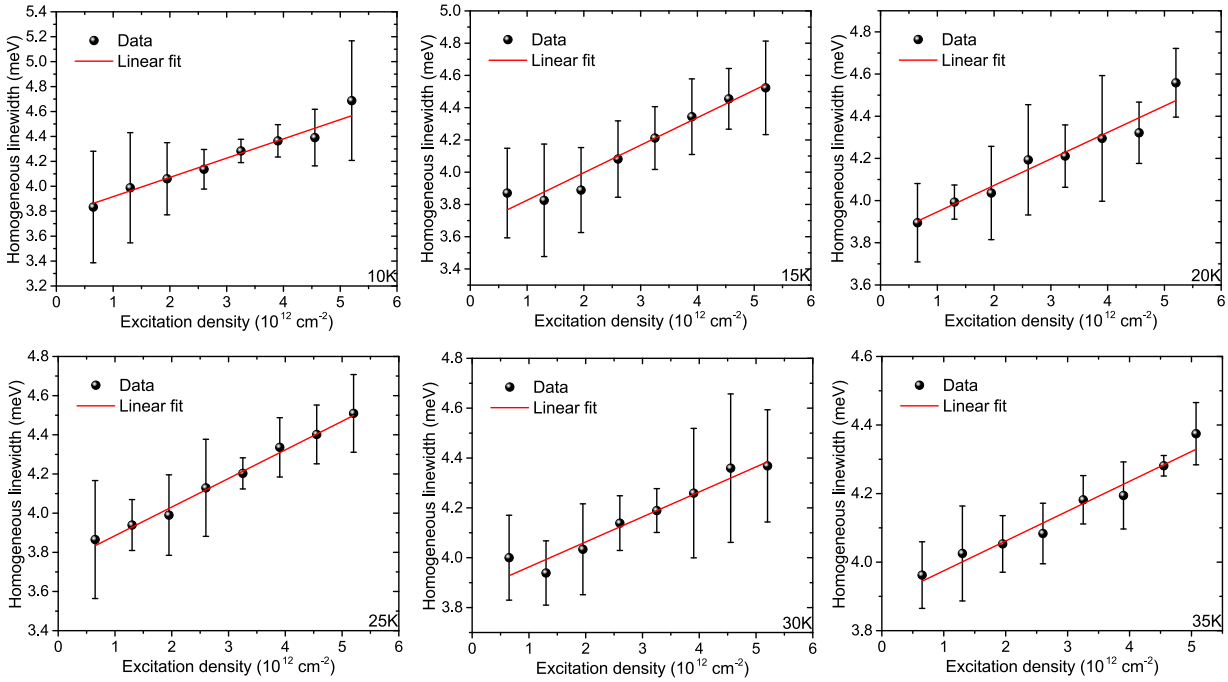

FIG. 4: Excitation density dependence of the homogeneous linewidth at various temperatures. The extrapolated homogeneous linewidths at zero excitation density are used in Figure 3(c) in the main text. The red lines are linear fit.

* Email address: hebin.li@fiu.edu

[1] Q. H. Wang, K. Kalantar-Zadeh, A. Kis, J. N. Coleman, and M. S. Strano, Nat. Nanotechnol. **7**, 699 (2012).
[2] X. Xu, W. Yao, D. Xiao, and T. F. Heinz, Nat. Phys. **10**, 343 (2014).
[3] D. Xiao, G. B. Liu, W. Feng, X. Xu, and W. Yao, Phys. Rev. Lett. **108**, 196802 (2012).
[4] Z. Ye, D. Sun, and T. F. Heinz, Nat. Phys. **1**, 1 (2016).
[5] O. Gunawan, B. Habib, E. P. De Poortere, and M. Shayegan, Phys. Rev. B **74**, 155436 (2006).
[6] A. Rycerz, J. Tworzydlo, and C. W. J. Beenakker, Nat. Phys. **3**, 172 (2007).
[7] D. Xiao, W. Yao, and Q. Niu, Phys. Rev. Lett. **99**, 236809 (2007).
[8] W. Yao, D. Xiao, and Q. Niu, Phys. Rev. B **77**, 235406 (2008).
[9] N. C. Bishop, M. Padmanabhan, K. Vakili, Y. P. Shkolnikov, E. P. De Poortere, and M. Shayegan, Phys. Rev. Lett. **98**, 266404 (2007).
[10] Y. P. Shkolnikov, E. P. De Poortere, E. Tutuc, and M. Shayegan, Phys. Rev. Lett. **89**, 226805 (2002).
[11] C. H. Bennett and D. P. DiVincenzo, Nature **404**, 247 (2000).
[12] G. D. Scholes, G. R. Fleming, L. X. Chen, A. Aspuru-Guzik, A. Buchleitner, D. F. Coker, G. S. Engel, R. van Grondelle, A. Ishizaki, D. M. Jonas, et al., Nature **543**, 647 (2017).
[13] T. Korn, S. Heydrich, M. Hirmer, J. Schmutzler, and C. Schu?ller, Appl. Phys. Lett. **99**, 102109 (2011).
[14] D. Lagarde, L. Bouet, X. Marie, C. R. Zhu, B. L. Liu, T. Amand, P. H. Tan, and B. Urbaszek, Phys. Rev. Lett. **112**, 047401 (2014).
[15] H. Shi, R. Yan, S. Bertolazzi, J. Brivio, B. Gao, A. Kis, D. Jena, H. G. Xing, and L. Huang, ACS Nano **7**, 1072 (2013).
[16] Q. Wang, S. Ge, X. Li, J. Qiu, Y. Ji, J. Feng, and D. Sun, ACS Nano **7**, 11087 (2013).
[17] C. Mai, A. Barrette, Y. Yu, Y. G. Semenov, K. W. Kim, L. Cao, and K. Gundogdu, Nano Lett. **14**, 202 (2014).
[18] C. Mai, Y. G. Semenov, A. Barrette, Y. Yu, Z. Jin, L. Cao, K. W. Kim, and K. Gundogdu, Phys. Rev. B **90**, 041414 (2014).
[19] E. M. Mannebach, K.-A. N. Duerloo, L. A. Pellouchoud, M.-J. Sher, S. Nah, Y.-H. Kuo, Y. Yu, A. F. Marshall, L. Cao, E. J. Reed, et al., ACS Nano **8**, 10734 (2014).
[20] H. Wang, C. Zhang, and F. Rana, Nano Lett. **15**, 339 (2015).
[21] G. Moody, J. Schaibley, and X. Xu, J. Opt. Soc. Am. B **33**, C39 (2016).
[22] A. D. Bristow, D. Karaiskaj, X. Dai, T. Zhang, C. Carlsson, K. R. Hagen, R. Jimenez, and S. T. Cundiff, Rev. Sci. Instrum. **80**, 073108 (2009).
[23] H. Li, G. Moody, and S. T. Cundiff, Opt. Express **21**, 1687 (2013).
[24] M. E. Siemens, G. Moody, H. Li, A. D. Bristow, and S. T. Cundiff, Opt. Express **18**, 17699 (2010).
[25] X. Dai, M. Richter, H. Li, A. D. Bristow, C. Falvo, S. Mukamel, and S. T. Cundiff, Phys. Rev. Lett. **108**, 193201 (2012).
[26] F. Gao, S. T. Cundiff, and H. Li, Opt. Lett. **41**, 2954 (2016).
[27] T. Brixner, J. Stenger, H. M. Vaswani, M. Cho, R. E.

Blankenship, and G. R. Fleming, Nature **434**, 625 (2005).
[28] G. S. Engel, T. R. Calhoun, E. L. Read, T.-K. Ahn, T. Mančal, Y.-C. Cheng, R. E. Blankenship, and G. R. Fleming, Nature **446**, 782 (2007).
[29] D. Turner, P. Wen, D. Arias, K. Nelson, H. Li, G. Moody, M. Siemens, and S. Cundiff, Phys. Rev. B **85**, 201303 (2012).
[30] R. Singh, T. M. Autry, G. Nardin, G. Moody, H. Li, K. Pierz, M. Bieler, and S. T. Cundiff, Phys. Rev. B **88**, 45304 (2013).
[31] G. Nardin, G. Moody, R. Singh, T. M. Autry, H. Li, F. Morier-Genoud, and S. T. Cundiff, Phys. Rev. Lett. **112**, 046402 (2014).
[32] G. Moody, I. A. Akimov, H. Li, R. Singh, D. R. Yakovlev, G. Karczewski, M. Wiater, T. Wojtowicz, M. Bayer, and S. T. Cundiff, Phys. Rev. Lett. **112**, 97401 (2014).
[33] G. Moody, R. Singh, H. Li, I. A. Akimov, M. Bayer, D. Reuter, A. D. Wieck, A. S. Bracker, D. Gammon, and S. T. Cundiff, Phys. Rev. B **87**, 41304 (2013).
[34] G. Moody, R. Singh, H. Li, I. A. Akimov, M. Bayer, D. Reuter, A. D. Wieck, and S. T. Cundiff, Phys. Rev. B **87**, 045313 (2013).
[35] G. Moody, C. Kavir Dass, K. Hao, C.-H. Chen, L.-J. Li, A. Singh, K. Tran, G. Clark, X. Xu, G. Berghäuser, et al., Nat. Commun. **6**, 8315 (2015).
[36] K. Hao, L. Xu, P. Nagler, A. Singh, K. Tran, C. K. Dass, C. Schüller, T. Korn, X. Li, and G. Moody, Nano Lett. **16**, 5109 (2016).
[37] K. Hao, G. Moody, F. Wu, C. K. Dass, L. Xu, C.-H. Chen, L. Sun, M.-Y. Li, L.-J. Li, A. H. MacDonald, et al., Nat. Phys. **12**, 677 (2016).
[38] K. Hao, J. F. Specht, P. Nagler, L. Xu, K. Tran, A. Singh, C. K. Dass, C. Schüller, T. Korn, M. Richter, et al., Nat. Commun. **8**, 15552 (2017).
[39] K. Hao, L. Xu, F. Wu, P. Nagler, K. Tran, X. Ma, C. Schüller, T. Korn, A. H. MacDonald, G. Moody, et al., 2D Materials **4**, 025105 (2017).
[40] M. A. Lampert, Phys. Rev. Lett. **1**, 450 (1958).
[41] K. Kheng, R. T. Cox, M. Y. d' Aubigné, F. Bassani, K. Saminadayar, and S. Tatarenko, Phys. Rev. Lett. **71**, 1752 (1993).
[42] A. M. Jones, H. Yu, N. J. Ghimire, S. Wu, G. Aivazian, J. S. Ross, B. Zhao, J. Yan, D. G. Mandrus, D. Xiao, et al., Nat. Nanotechnol. **8**, 634 (2013).
[43] J. S. Ross, S. Wu, H. Yu, N. J. Ghimire, A. M. Jones, G. Aivazian, J. Yan, D. G. Mandrus, D. Xiao, W. Yao, et al., Nat. Commun. **4**, 1474 (2013).
[44] K. F. Mak, K. He, C. Lee, G. H. Lee, J. Hone, T. F. Heinz, and J. Shan, Nat. Mater. **12**, 207 (2012).
[45] C. H. Lui, A. J. Frenzel, D. V. Pilon, Y.-H. Lee, X. Ling, G. M. Akselrod, J. Kong, and N. Gedik, Phys. Rev. Lett. **113**, 166801 (2014).
[46] A. M. Jones, H. Yu, J. R. Schaibley, J. Yan, D. G. Mandrus, T. Taniguchi, K. Watanabe, H. Dery, W. Yao, and X. Xu, Nat. Phys. **12**, 323 (2015).
[47] A. Singh, G. Moody, S. Wu, Y. Wu, N. J. Ghimire, J. Yan, D. G. Mandrus, X. Xu, and X. Li, Phys. Rev. Lett. **112**, 216804 (2014).
[48] A. Singh, G. Moody, K. Tran, M. E. Scott, V. Overbeck, G. Berghäuser, J. Schaibley, E. J. Seifert, D. Pleskot, N. M. Gabor, et al., Phys. Rev. B **93**, 041401 (2016).
[49] F. Gao, Y. Gong, M. Titze, R. Almeida, P. M. Ajayan, and H. Li, Phys. Rev. B **94**, 245413 (2016).
[50] G. Wang, L. Bouet, D. Lagarde, M. Vidal, A. Balocchi, T. Amand, X. Marie, and B. Urbaszek, Phys. Rev. B **90**, 075413 (2014).
[51] X. Wang, Y. Gong, G. Shi, W. L. Chow, K. Keyshar, G. Ye, R. Vajtai, J. Lou, Z. Liu, E. Ringe, et al., ACS Nano **8**, 5125 (2014).
[52] W. Wagner, C. Li, J. Semmlow, and W. S. Warren, Opt. Express **13**, 3697 (2005).
[53] H. Wang, K. Ferrio, D. G. Steel, Y. Z. Hu, R. Binder, and S. W. Koch, Phys. Rev. Lett. **71**, 1261 (1993).
[54] C. L. Smallwood, T. M. Autry, and S. T. Cundiff, J. Opt. Soc. Am. B **34**, 419 (2017).
[55] V. Perlík, J. Hauer, and F. Šanda, J. Opt. Soc. Am. B **34**, 430 (2017).
[56] A. Honold, L. Schultheis, J. Kuhl, and C. W. Tu, Phys. Rev. B **40**, 6442 (1989).
[57] P. Dey, J. Paul, Z. Wang, C. E. Stevens, C. Liu, A. H. Romero, J. Shan, D. J. Hilton, and D. Karaiskaj, Phys. Rev. Lett. **116**, 127402 (2016).
[58] H. P. Wagner, A. Schätz, R. Maier, W. Langbein, and J. M. Hvam, Phys. Rev. B **56**, 12581 (1997).
[59] M. Selig, G. Berghuser, A. Raja, P. Nagler, C. Schller, T. F. Heinz, T. Korn, A. Chernikov, E. Malic, and A. Knorr, Nat. Commun. **7**, 13279 (2016).
[60] Z. Lin, B. R. Carvalho, E. Kahn, R. Lv, R. Rao, H. Terrones, M. A. Pimenta, and M. Terrones, 2D Materials **3**, 022002 (2016).